

AUTOMATED MANUFACTURING OF GRID STIFFENED PANELS WITH RADICALLY REDUCED TOOLING

Harry Ratkai, Sumaiya S. Tanu, Donald W. Radford
Composite Materials, Manufacture and Structures Laboratory
Colorado State University
Fort Collins, Colorado, USA

ABSTRACT

Grid stiffened continuous fiber reinforced composite panels are an attractive option for creating lightweight structures due to the tailorability for various applications and the resulting high specific properties. However, the panel stiffeners and stiffener intersections result in high tooling complexity and correspondingly high cost of implementation. These factors have limited the impact of such structures in the composites industry. Previous research has demonstrated the ability to produce high quality, high aspect ratio beams, representative of individual grid stiffeners, using E-glass/PET comingled tow via direct digital manufacturing. Further, prior preliminary efforts have demonstrated the potential to use the same approach to manufacture grid intersections that have continuous fiber in both directions. To expand on the previous efforts in grid stiffeners produced by direct digital manufacture with radically reduced tooling requirements, this effort compares two methods of providing positioning and consolidation, nozzle vs. roller. Both processes are based on a commingled yarn feedstock. The extrusion through a nozzle has been shown to enable grid intersection control through local variations in applied consolidation and serves as the baseline process. However, this approach requires a continuous placement path to create the complete grid stiffened panel as no mechanism for cutting and restarting has been implemented. Alternatively, a newly developed placement head incorporating cut and refeed, mounted to a 6-axis robot, offers the potential of improved path placement efficiency. The two techniques are used to produce similar grid composite stiffeners to evaluate the effectiveness of producing the grid intersections. Rate of deposition of the two end effectors are compared and the quality of the associated grid stiffeners, and intersections, are determined through measurement of geometry, fiber volume fraction and void fraction.

Keywords: Grid Stiffeners; Consolidation; Glass Fiber; Thermoplastic Composites; Voids.

1. INTRODUCTION

Grid stiffened structures have long been used as a method for lightweighting. Traditionally machined out of an aluminum billet, fiber reinforced composite grid stiffened structures are very attractive for such a design based on the high specific properties and greater tailorability of the reinforcing fibers. Additionally, grid stiffened structures show good damage tolerance and load path redundancy [1]. However, manufacturing composite grid stiffened structures is not without issues. Design, manufacturing, cost, quality control, and a relative lack of knowledge about these structures have made it difficult for industry to adopt, mature, and implement composite grid stiffened components.

One issue with manufacturing continuous fiber composite grid stiffened structures is build-up of the reinforcement at the intersection points; where there is twice as much fiber at the crossover point as in the straight rib sections. The material and thickness build-up at the intersections leads to fiber bridging which in turn leads to resin rich areas, before and after the crossing plies. The ribs, before and after these intersections, were the failure sites when Buragohain et al. performed compression testing on a cylindrical lattice structure [2]. Traditional manufacturing methods of composite grid stiffened structures rely on the expansion of the specialty tooling to provide lateral compaction of the ribs [3]. While this improves the mechanical properties and in-plane geometric control, it does not address the thickness deviations at the crossover points. Zhao et al., made grid stiffened structures using Automated Fiber Placement (AFP) and attempted to decrease the fiber waviness at the nodal intersections by introducing discontinuous tows at the crossover points. While this reduced the thickness differences between the ribs and intersections, the introduction of discontinuous tows did drop the compressive and bending properties [4]. Lee et al. proposed a rib compression method using rollers to minimize voids and fiber spreading in the thickness direction at resin rich areas [5].

Another issue with the manufacture of composite grid stiffened structures is the required tooling complexity. The earliest method of manufacturing tooling for grid stiffened panels was either by milling or fabrication of aluminum. Buragohain et al. used a polyurethane (PU) foam mandrel with grooves machined into it. Not only was the tool sacrificial, but the use of a 4-axis mill was necessitated [2]. Ahmadi et al. created an isogrid mesh by dry weaving fiber roving along the grooves of a silicon mold and then filled the grooves with epoxy resin [6]. This approach has the disadvantage that when the stacked fiber height exceeds the silicon guide, the fiber slips over the silicon guide and spreads out. Lee et al. prevented this by using an adhesive like paper tape to hold the fiber near the silicon guide, preventing the fiber from spreading [5]. When using expansion block tooling, each block is machined individually and sized carefully, or is cast in high tolerance tooling, to ensure part quality. Improper fabrication can cause higher loads to concentrate at the intersections. Vacuum assisted resin transfer molding has also been an alternative used to manufacture grid-stiffened panels, but this method is costly for long composites parts due to the two-sided, closed mold requirement and due to the number of fixtures required in the process [7].

1.1 Digital Manufacturing

Costly ‘trial and error’ can be avoided, and the scrap rate can be minimized, by employing fiber placement heads with advanced capabilities and variable tow width handling in automated methods of fiber deposition. Two primary technologies: AFP and Automated Tape Laying (ATL) use pre-impregnated fiber tows that can be placed or stacked to construct a grid of the required height. Compared to traditional manufacturing processes, these methods offer quality, stability and placement efficiency [8]. Additionally, automated placement methods enable cost-effective production of large, complex, and high-quality components in a single step. However, in order to avoid fiber bridging during AFP, Netherlands Aerospace Center (NRL) demonstrated that cutting half of the tapes in one direction and the other half in the opposite direction at the intersections of orthogrid stiffeners was necessary [9]. Unfortunately, this results in a more complex grid intersection design and negatively affects the fiber continuity.

Previous work has demonstrated the manufacturing of high quality, high fiber volume fraction grid stiffener beams by direct digital manufacture with radically reduced tooling requirements. This research by Hogan et al. demonstrated the use of continuous fiber reinforced thermoplastic commingled tow to produce multi-layer, high aspect ratio grid stiffener beams directly on a tool surface without any channels or guides [11]. A fiber volume fraction in excess of 50% was reported, using a commingled glass/PET. In follow-on work by Hogan, it was determined that tow spreading, and ultimately tow thickness, could be effectively controlled through the variation of consolidation force of the hot nozzle used for the deposition of the commingled tow [12]. Further, this research culminated in the demonstration of grid intersections, which, through the local control of the processing parameters, had nearly equal thicknesses in the intersection and in the straight stiffener region, as shown in figure 1. The maintenance of thickness throughout the demonstration intersection, produced by Hogan [12], relied on local spreading and thinning during placement which yielded both a higher local fiber volume fraction at the crossover and a widening through local tow spreading.

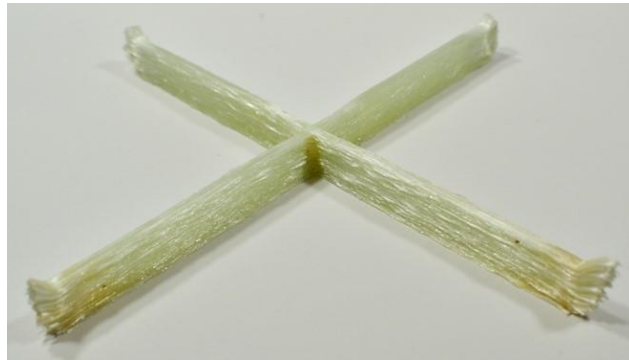


Figure 1: 40 layer stiffener grid intersection demonstration [12].

The current work compares two methods of direct digital continuous fiber positioning and consolidation of commingled continuous fiber reinforced thermoplastic feedstock; (i) a nozzle using the same system as used to produce the crossover demonstration of figure 1, and (ii) a heated roller. It is predicted that similar quality can be generated, in the straight stiffener, with the consolidation roller versus the nozzle. However, since the processed tow width is greater when using the consolidation roller there is a concern whether sufficient tow spreading can be introduced to maintain the equivalent thickness in the intersection as in the straight stiffener. This effort is also a preliminary demonstration of the ability to automate the cut and refeed process and thus, manufacture the composite grid stiffeners with less material waste and at higher deposition rates.

2. EXPERIMENTATION

This study compares the quality of the grid stiffeners, and grid stiffener intersections, manufactured using a gantry fiber deposition system (baseline nozzle consolidation process) and a 6-axis robot system with a roller consolidation end effector. In order to facilitate an effective comparison between the two cases, the geometry of the part was designed and characterized such that the stacking sequence of the grid at the intersection was $[(0/90)_{20}]$ and the number of tows placed are the same between the two systems. The placement systems were utilized to each generate two samples. One sample was printed at a deposition rate of 50 mm/min, while the other was printed at 300 mm/min. These speeds were chosen based on experience with rates used

successfully with the nozzle-based system, and are lower than the maximum speeds of the robot mounted roller consolidation system.

2.1 Materials

The commingled tow feedstock used in this study is Compofil PP-60-R-1870N (Fiberglass Industries Twintex), a continuous E-glass/Polypropylene (EG/PP) untwisted commingled tow. The Tex of the roving is 1870. The unprocessed weight fraction of the reinforcement is 60%, which corresponds to a 35% fiber volume fraction. Warlick et al., used the same material and reported the glass transition temperature of the PP polymer in the commingled tow to be below 0°C and the main melting peak, via differential scanning calorimetry (DSC), at a temperature of 163.8°C (327°F) [13]. The processing temperature for the heated zone of each end effector is set to a fixed, predetermined, 250°C based on prior processing experience. A low-tack adhesive backed PP tape was placed on top of the glass build plate to improve the bed adhesion of the commingled tow and to maintain the as-printed position on the substrate. The unprocessed commingled tow width is approximately 6 mm.

2.2 Nozzle Consolidation Fiber Deposition System

A custom gantry-based fiber deposition system was purpose-built to manufacture complex geometries and high fiber volume fraction structures, as shown in figure 2(a). This system has two print heads - one for the placement of conventional thermoplastic 3D printing filament and the other for the processing of continuous fiber reinforced composite materials in a manner similar to pultrusion, allowing the commingled tow to be pulled through a short, heated zone and custom designed nozzle. This work will make use of only the continuous fiber print head, as shown in figure 2(b).

The additional components added to the common FFF (Fused Filament Fabrication) hot end used as the basis for the continuous fiber processing print head consist of a custom fiber placement nozzle, cooling manifold, and spring-loaded consolidation system. A brass nozzle of 1.5 mm (0.059") inside diameter and 7 mm (0.276") outside diameter, shown in figure 2(b), was designed to allow for a single tow of commingled material to be compacted as it is being pulled through the nozzle, and then consolidated between the nozzle face and the previous surface. The outside diameter of the face of the nozzle is manufactured to be greater than the width of the spread commingled tow. For this nozzle-based process, the tow is shaped as it moves through the nozzle, to approximately the nozzle dimensions, and is then spread under the nozzle face. This results in a processed tow width narrower than that of the original 6 mm tow. A cooling manifold is attached to the end effector with two adjustable ducts for computer-controlled compressed air flow to locally cool and rapidly rigidize the newly placed composite. Warlick et al. developed this cooling system to increase positional fidelity when tow shearing of continuous fiber reinforced thermoplastic composite (CFRTC), using EG/PP, was implemented to enable enhanced tow steering [13]. By switching the cooling air on and off for localized cooling, this feature provides advantages of enhanced tow spreading and consolidation during programmed manufacture.

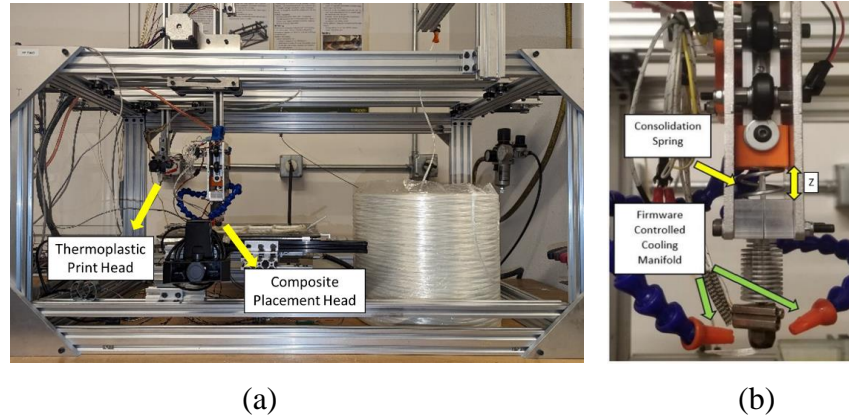


Figure 2: (a) Gantry fiber deposition system setup and (b) composite placement head. [11]

In order to improve consolidation quality and uniformity over surface variations and to eliminate voids, Rodriguez et al. [10] included a spring-loaded system which supports the nozzle. This spring-loaded end effector has a spring constant of approximately 7.5 N/mm which results in the application of a repeatable consolidation force on the placed tows. The amount of force applied is controlled by positioning the nozzle in the build direction (Z axis) at a height above the previous position such that a known amount of spring compression is introduced. To reduce the thickness of the composite tow and increase the tow width, it is possible to program a negative height value in relation to the build plate which results in a greater spring displacement and a correspondingly greater force. This enables the nozzle to exert pressure on the build plate, or on previously positioned tows, and spread the tows being currently placed. Load cells in the dual gantry system, supporting the build plate, are available to monitor the resultant consolidation force while continuous fiber placement is underway.

2.2.1 Sample Preparation for Nozzle-Based System

To manufacture grid stiffeners and grid intersections, a similar approach to that described by Hogan et al. was used to generate a continuous print path incorporating loops outside the basic stiffener profile [11]. The benefit of this approach is that it avoids the need to manually cut and restart the fibers after each layer is printed as was the case for the demonstration intersection shown in figure 1. This is convenient as multilayer grid stiffener specimens can take many hours to produce and the use of a continuous path removes the need for operator intervention. The deposition path program and toolpaths were defined using CAD software. Once the coordinates of the first layer are generated within the software, the X and Y coordinates are transferred to FullControl GCode Designer [17] to generate the points for the subsequent layers of the part without having to manually change the Z position for every layer. The layer height, or Z step, was set to a predetermined 0.3 mm. The consolidation of the layers is controlled by controlling the Z position of the gantry system. The initial Z position of the system is set by reading a force output from load cells installed under the build plate. The value for these tests was set to 11N, enabling the initial layer to effectively tack to the build plate. With a goal of a uniform grid height at the intersections, even with the local doubling of fiber count, the consolidation force, at the crossover region, the Z step was programmed to a value consistent with a 22N force. The higher consolidation force at the grid intersections allows for the tows to spread out, thus reducing the individual layer thickness, as depicted in figure 3.

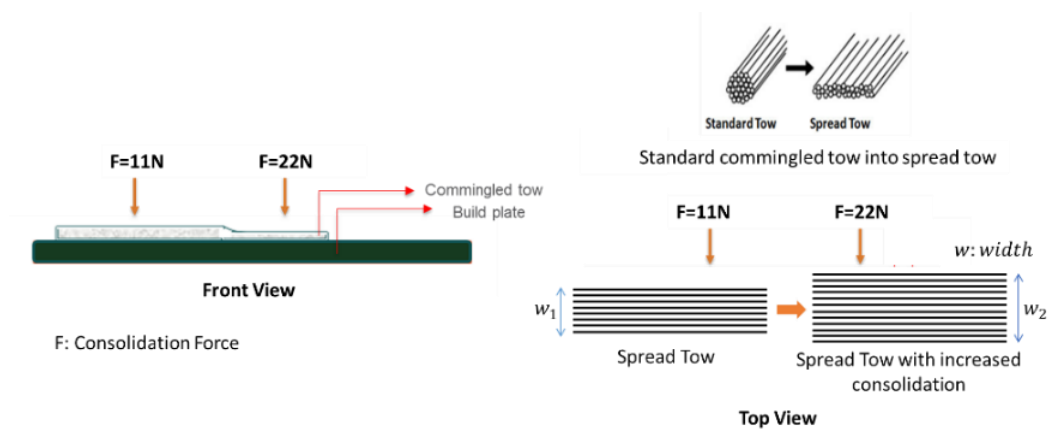


Figure 3: Image of spread of commingled yarn: Front view (left) and top view (right).^[14]

The specific continuous tool path used to create the reinforcing grids for the samples of this work is shown in figure 4. Only the straight regions adjacent to the 3 intersections and the intersections themselves are used in this effort.

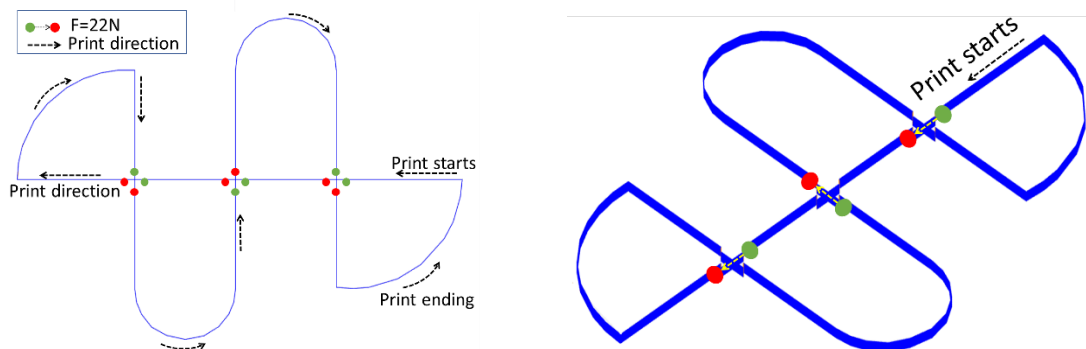


Figure 4: Continuous print path planning on single layer (left) and 20 layers generated using FullControl GCode Designer (right).

2.3 Roller Consolidation Fiber Deposition System

Due to the limitations of the gantry-mounted nozzle consolidation fiber deposition system in terms of speed and the required manual starting/stopping, a new continuous fiber deposition head was designed to be integrated with an ABB IRB4600 6-axis robot. The new deposition head includes a heated roller and a cut and refeed system to increase the deposition rate and to automate the stopping and starting of the composite placement, negating the need for the continuous paths described for the nozzle consolidation system.

The roller consolidation system consists of a 31.8 mm (1.25”) diameter, heated steel roller with two internal plain bearings. Through the center of the roller is a hollow shaft that accepts two 40W cartridge heaters. An infrared (IR) thermometer, DF Robot SEN 0256, is used to sense the temperature of the roller consolidation surface and enable temperature control using an Arduino Uno Rev 3 operating through a solid-state relay. The system is shown in figure 5(a). The cut and refeed subsystem consists of a spring actuated anvil roller, a driven cutting roller, similar to that used in a composite chopper gun, a cam, and a roller follower. Portions of the cut and refeed

system can be seen in figure 5(b). This cut and refeed system, in concept, allows the tow to be cut while the placement head is still in motion; however, in practice, the system motion rate is reduced during the cut and refeed process.

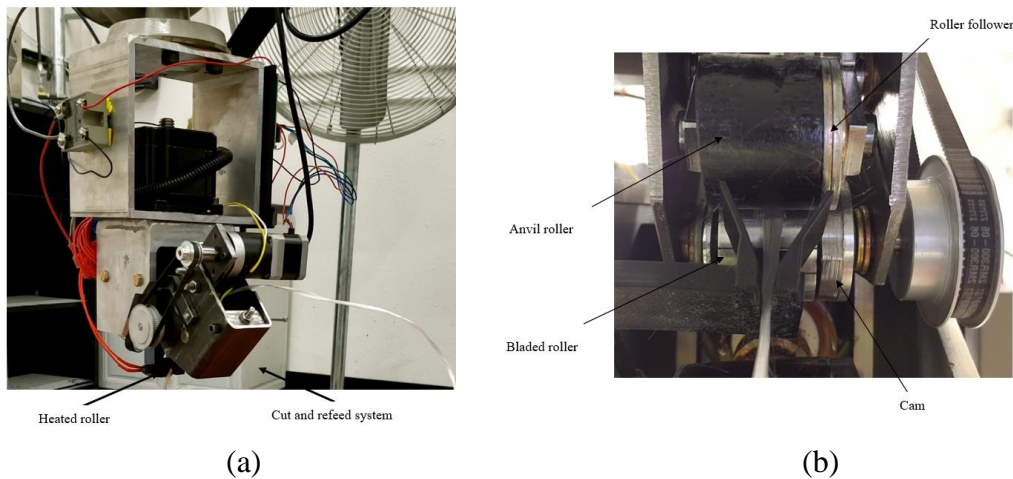


Figure 5: (a) The Deposition Head and (b) the Cut and Refeed System.

Differences between the gantry deposition and robotic deposition include the method of consolidation, ability to automatically cut and refeed, stiffness of each system and load monitoring. The gantry system uses a heated nozzle to initially form the tow into a cylindrical cross section and then presses the shaped tow into a rectangular "tape". Further, the gantry system has no ability to automatically cut and refeed the fibers; all stopping and starting is a manual process. The gantry system does have a spring integrated into the nozzle, enabling a more consistent application of the consolidation force and less affect from deviations in the bed flatness and levelness. Finally, the gantry system has load cells supporting the print bed, enabling load monitoring during printing. The robotic system deposits the tow using a heated roller and the commingled feedstock is introduced in the original form and is directly deposited as a "tape". This results in a greater placed tow width than the nozzle consolidation system, for a given consolidation force. The robotic deposition system has no spring integrated into the system, yielding a stiffer system and less tolerance for bed variations from level. Finally, this research was performed before force monitoring and feedback capabilities were implemented in the robotic system.

2.3.1 Sample Preparation for the Robot-Based Process

The samples, using the robot, were printed on a sheet of glass secured to a stationary turntable. The roller temperature was set at 250°C in an attempt to match the parameter used in the nozzle-based process, and the layer height was set at 0.15 mm. The reduced layer height, compared to the nozzle-based system, is necessitated by the difference in tow geometry prior to consolidation. For the crossover, the robot displaces an additional -0.1 mm in the Z direction to increase consolidation force and, as a result, spread and thin the tow. The print speed was set to 300 mm/min for one sample and 50 mm/min for the second sample, matching the placement speeds of the nozzle-based system. Both samples had 20 layers in the beam sections and 40 layers at the crossovers.

To program the print path for the ABB robot, the centerlines of each single layer were created in CAD and were then exported to a commercial robot simulation software. The path was aligned

with the X and Y axes to make the code more intuitive and easier to read. To find the correct User and WorkObject coordinate systems, the robot was manually jogged to the start/stop locations of the X and Y paths and the crossover point. At each of these points, the robot was jogged along the Z axis until the roller was in slight contact with a piece of 0.10 mm (0.004”) shim stock; the height was then recorded, and the coordinate system was reoriented accordingly to account for build plate variations from level. Due to variations in the levelness of the print bed, some manipulation of the print path was needed as compensation. This manipulation is summarized in Table 1. The same compensation was applied to, and verified for, all three paths in the Y direction. A “FOR” loop was then used to step the robot through the print path, in a layer-wise fashion.

TABLE 1: Z Height Compensation in the Print Paths

	Z height (mm)		Z height (mm)
Xstart	0.2	Ystart	0.3
Crossover	0	Crossover	0
Xstop	0.2	Ystop	0.1

2.4 Specimen Evaluation Procedures

The four samples were evaluated for thickness variations, both within the straight grid stiffeners and at the crossovers and were then sectioned to enable local fiber and void fraction determination.

2.4.1 Geometry Measurement Procedure

The quality of the fabricated parts was investigated by measuring the variation in the 20 layer height over the length of the straight beam (X, Y1, Y2 and Y3) sections as well as in the 40 layer crossovers (C1, C2 and C3), as shown in figure 6. The geometry of each specimen was measured 3 times at each of the locations, using a micrometer, prior to sectioning.

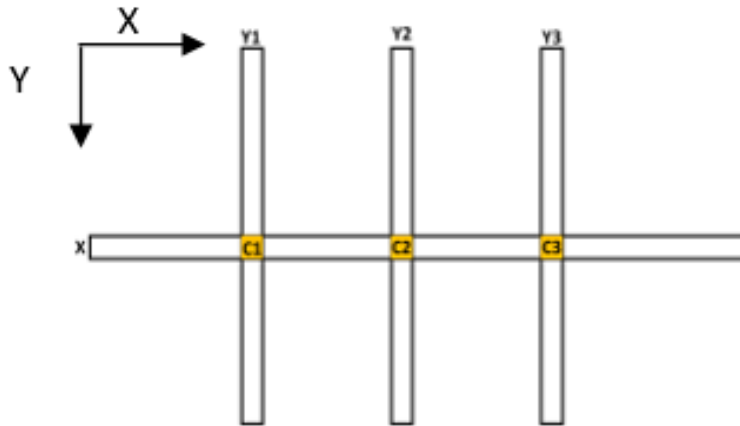


Figure 6: Image of sample and labeling. From left to right: Y1, Y2, and Y3.

Samples from each manufacturing system are shown in figure 7. The differences outside the areas to be analyzed are clear, with the full continuous path shown in figure 7(a) and the discrete path, which is the result of the added cut and refeed capabilities, in figure 7(b).

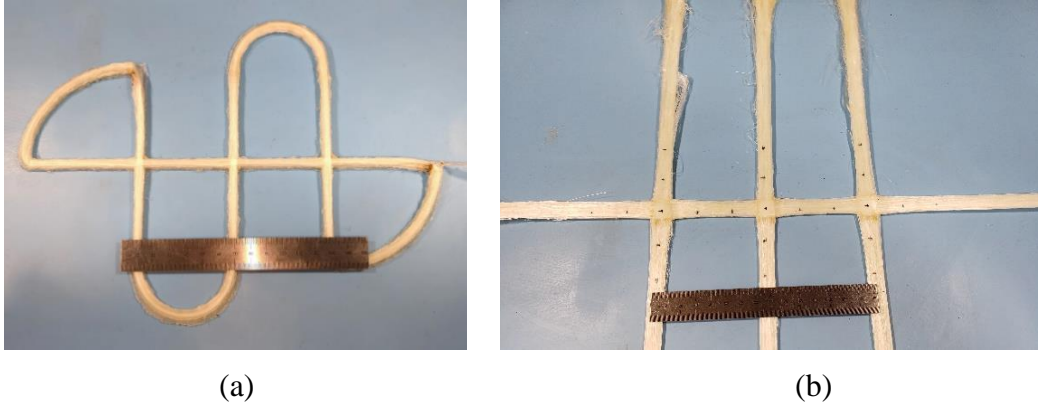


Figure 7: Examples of samples printed at 300 mm/min using, (a) the gantry-based nozzle consolidation system and (b) the robot-mounted roller consolidation system.

Also apparent is the difference in beam width of the two 20 layer specimens at the same 300 mm/minute deposition speed. Since the amount of fiber positioned by the two systems, in each layer, is identical, the greater width shown in figure 7(b) is consistent with a smaller layer thickness. Specifically, the thicknesses were evaluated at the positions indicated by the black dots visible in figure 7(b), corresponding to the three straight beams and crossovers labeled in figure 6.

2.4.2 Volume Fraction Determination

To prepare the specimens for quality evaluation, a water-cooled diamond saw was used to section the crossover regions from the grid stiffener beams produced by both placement systems. The sectioning was done at least 10 mm from the crossover region, and the straight beam specimens were cut to a length of 25 mm. This sectioning of the specimens is shown, for one of the roller consolidated specimens, in figure 8. To ensure consistency between specimens generated via the nozzle and roller deposition heads, 10 straight beams and 3 crossover specimens were prepared from each sample. No post-processing was performed on the samples in an attempt preserve the as-printed properties. The quality of the composite stiffener beams was analyzed by determination of the fiber volume fraction and the void volume fraction of both the straight beam and crossover specimens.

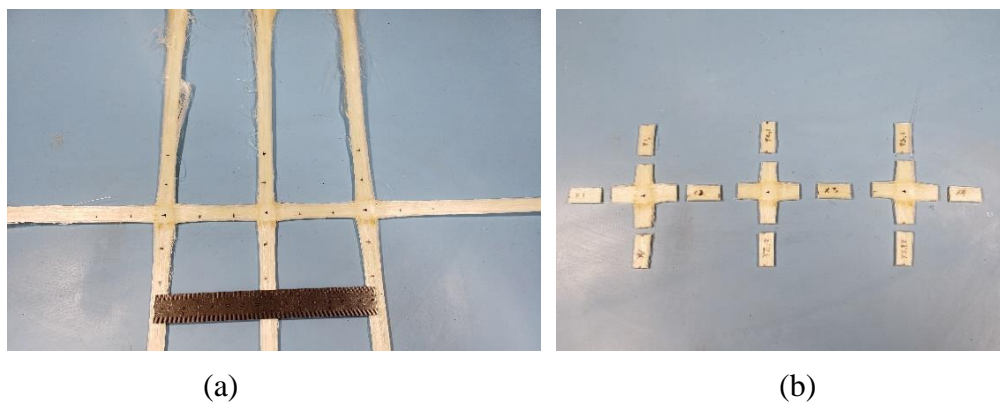


Figure 8: Examples of (a) a roller consolidated, 3 crossover sample before cutting and, (b) the associated specimens after cutting in preparation for volume fraction analysis.

To determine the void volume fraction of a specimen, the Archimedes principle was used to find the density. To determine the volume of each specimen, the fluid displacement method, based on ASTM 792, was used [15]. RedLine Water Wetter was used, in a ratio of 32:1 deionized (DI) water to RedLine, Water Wetter in order to minimize the bubble formation on the specimens and thus improve the accuracy of the measurement. To determine the weight fraction of fibers in each specimen, the matrix burn-off method was performed, according to ASTM D3171-15 [16]. To perform the matrix burn-off method, the specimens are first placed in a ceramic crucible and dried at 70°C in an oven with desiccant for an hour to reach equilibrium. Then, the specimens are put in the furnace, in air, and the temperature is set to 596°C for at least 4 hours to ensure complete removal of the matrix. The loose fibers are then weighed, allowing determination of both fiber and void volume fractions through the use of manufacturer supplied densities.

3. RESULTS

3.1 Geometry Measurements

Geometries were measured following the protocol and organization described in Section 2.4.1 and are presented separately for the two composite consolidation approaches.

3.1.1 Gantry Deposition

The variation in grid thickness over the length of the grid stiffeners and at the crossovers for the gantry deposition is given in Table 2.

TABLE 2: Summary of Thickness Measurements for the Gantry Deposition.

		X				
		X Avg. (mm)	% Standard Deviation	Crossover Average (mm)	% Crossover Deviation	% Programmed Deviation
Speed (mm/min)	300	5.686	5.00%	6.276	10.37%	5.23%
	50	4.366	0.88%	4.794	9.81%	27.23%
		Y1				
		Y1 Avg. (mm)	% Standard Deviation	C1 (mm)	% Crossover Deviation	% Programmed Deviation
Speed (mm/min)	300	5.761	5.21%	6.254	8.57%	3.99%
	50	4.509	0.72%	4.772	5.82%	24.85%
		Y2				
		Y2 Avg. (mm)	% Standard Deviation	C2 (mm)	% Crossover Deviation	% Programmed Deviation
Speed (mm/min)	300	5.457	5.50%	6.242	14.39%	9.05%
	50	4.267	1.91%	4.769	11.78%	28.89%
		Y3				
		Y3 Avg. (mm)	% Standard Deviation	C3 (mm)	% Crossover Deviation	% Programmed Deviation
Speed (mm/min)	300	5.628	4.88%	6.331	12.48%	6.19%
	50	4.442	1.03%	4.842	9.02%	25.98%

A comparison of the beams and crossovers, using % Crossover Deviation and % Programmed Deviation data, calculated from the thickness data, is also included in the tabulated data. The

% Crossover Deviation is the comparison of the straight beam section thickness to the crossover thickness. The % Programmed Deviation measures the difference between the average beam thickness and the programmed thickness of 6 mm, based on 20 layers, each with a layer height of 0.3 mm. From Table 2, it is observed that sample printed at 300 mm/min consistently shows a higher crossover thickness deviation than the sample printed at 50 mm/min. The average standard deviation of the beam thicknesses for the 300 mm/minute sample is 4 times higher than that of the sample printed at 50 mm/min. The increase in the standard deviation is likely caused by more limited matrix flow at the higher feed-rate. It is known that feed rate is related to the heat input to the tow as it determines the amount of time the commingled tow spends in the heated zone. Both samples are printed at the same nozzle temperature, 250°C, and the feed rate is the only controlled parameter that changes between the two placement speeds. Therefore, printing at a higher feed rate (6 times greater in speed in this case) means the commingled tow spends less time in the hot zone compared to sample printed at 50 mm/min. The higher placement speed not only reduces the actual tow temperature leaving the nozzle, resulting in a higher matrix viscosity, resisting flow, but also the duration of time the tow is under the nozzle is reduced, allowing less time for the matrix to flow under consolidation pressure and increase the width of the tow at the crossover. Furthermore, when printing in a continuous path and making sharp angle changes, the tow increases in thickness. At a faster deposition speed, the tow has less time to rigidize, leading to a more significant thickness deviation. As a result, the standard deviation of thickness in the sections printed at 300 mm/min is higher than that in the sections printed at 50 mm/min. This thickness deviation can be seen, graphically, in figure 9.

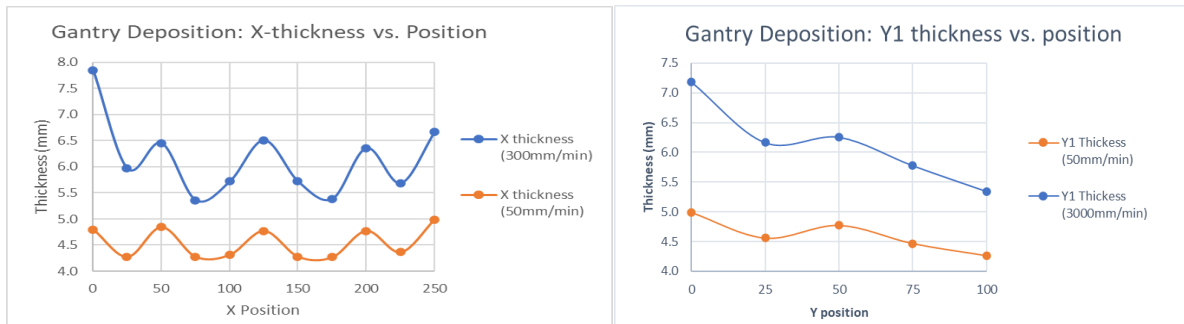


Figure 9: Graphical representation of X thickness variations (left) and representative graph of the Y thickness variation (right) for the gantry system.

The negative values for the % Programmed Deviation are due to the consolidation provided by the initial compression of the spring. The slower print speed allows the tow to spread more, allowing the spring to extend further and results in a greater deviation from the programmed height.

3.1.2 Robotic Deposition

Thickness measurements of the roller consolidated specimens are summarized in Table 3. Table 3 displays the average thickness of four beams (X, Y1, Y2, and Y3) and a comparison with the corresponding crossover values (C1, C2, and C3). The X-direction beam is compared with the average of the three crossovers as it is part of all three crossovers. To calculate the % Programmed Deviation, a programmed thickness of 3 mm was used.

TABLE 3: Summary of Thickness Measurements for Robotic Deposition.

		X				
		X Avg. (mm)	% Standard Deviation	Crossover Average (mm)	% Crossover Deviation	% Programmed Deviation
Speed (mm/min)	300	3.318	2.30%	3.482	4.93%	10.61%
	50	3.232	1.65%	3.182	-1.55%	7.73%
		Y1				
		Y1 Avg. (mm)	% Standard Deviation	C1 (mm)	% Crossover Deviation	% Programmed Deviation
Speed (mm/min)	300	3.197	3.82%	3.453	8.01%	6.56%
	50	3.162	4.22%	3.096	-2.08%	5.40%
		Y2				
		Y2 Avg. (mm)	% Standard Deviation	C2 (mm)	% Crossover Deviation	% Programmed Deviation
Speed (mm/min)	300	3.273	1.94%	3.517	7.45%	9.11%
	50	3.253	2.50%	3.214	-1.22%	8.45%
		Y3				
		Y3 Avg. (mm)	% Standard Deviation	C3 (mm)	% Crossover Deviation	% Programmed Deviation
Speed (mm/min)	300	3.272	1.97%	3.476	6.22%	9.08%
	50	3.227	1.92%	3.235	0.26%	7.56%

In general, the slower speed results in significantly better geometric control in the crossovers than the faster speed. This is not surprising as the matrix has more time to flow while under the pressure of the consolidation roller. Further, the matrix experiences the heat of the consolidation roller for longer, allowing more heat to transfer into the matrix. This, in turn, lowers the viscosity of the matrix, allowing more flow to take place. The thickness of the X-direction beams and of the crossovers is depicted in figure 10 and a clear trend is apparent. The sample printed at 300 mm/min has local thickness maximums at the crossover points, whereas the sample printed at 50 mm/min has local minimums at the crossover points. This is due to additional tow spreading, consistent with a longer time under the heated roller.

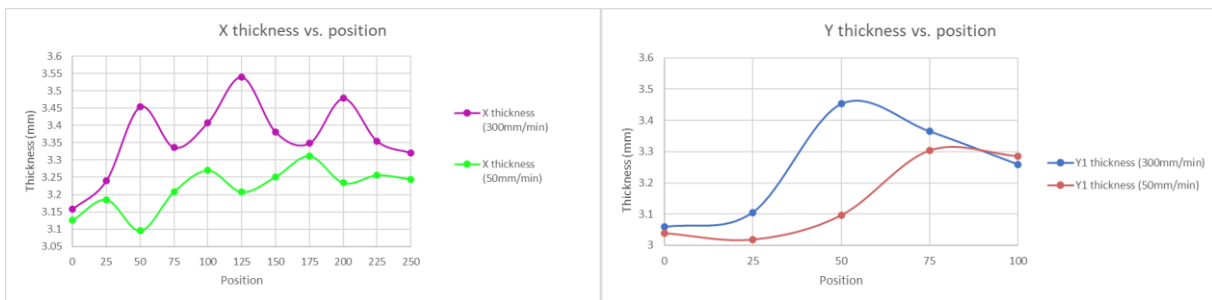


Figure 10: Graphical representation of X thickness variations (left) and representative graph of the Y thickness variation (right) for the robotic system.

One trend for the robotic deposition system is the general increase in thickness with an increase in position for both X and Y, as shown in figure 10. An explanation is related to imperfect bed leveling and height compensation.

3.2 Volume Fraction Analysis

In addition to the geometry analysis, fiber and void volume fractions of the composite samples were measured, using the approach detailed in Section 2.4.2, at several locations, as shown in figure 8. The specimens were used to calculate the average for both the straight beam and crossover regions.

3.2.1 Gantry Deposition

The fiber and void fractions of the gantry deposition system are summarized in Table 4. As previously stated, the unprocessed commingled EG/PP tow contains 35% fiber volume fraction. The crossover specimens have a higher fiber volume fraction compared to that of the beam specimens. It is particularly evident in the case of the sample printed at a speed of 50 mm/min, which exhibits superior quality, with a fiber volume fraction of 45.5% and void fraction of 7.12%. This is primarily due to the doubling of fiber in the crossover regions, which results in a greater amount of fiber being packed into a given laminate volume.

In Section 3.1.1, the geometry analysis revealed that the sample printed at a speed of 300 mm/min had lower geometric fidelity than the one printed at 50 mm/min. For the sample printed at a higher speed, the tow spent less time in the heated zone of the nozzle and under the consolidation face, limiting the heat into the tow and the resultant flow and subsequent spreading. Consequently, there is less time for flattening the tow and voids are not squeezed out of the laminate effectively. This leads to the accumulation of voids within the laminate due to the entrapment of air and moisture, resulting in a higher void volume fraction for sample printed at 300 mm/min.

TABLE 4: Average Fiber and Void Fraction Determined at Crossovers, X and Y Positions (Gantry)

		X		Y1		Y2		Y3		Beam		Crossover	
		Ave (%)	SD (%)	Ave (%)	SD (%)	Ave (%)	SD (%)	Ave (%)	SD (%)	Ave (%)	SD (%)	Ave (%)	SD (%)
300mm/ min	V_f	32.48	0.53	31.22	0.96	31.83	0.64	33.11	0.56	32.16	0.67	36.07	0.69
	V_v	7.53	0.28	13.58	2.10	7.04	0.52	5.62	0.43	8.44	0.58	13.58	0.87
50mm/ min	V_f	35.26	0.79	34.42	0.68	36.03	0.54	34.35	0.62	35.01	0.66	45.51	0.66
	V_v	3.11	0.63	5.42	0.37	2.40	0.39	2.93	0.45	3.46	0.46	7.12	0.46

3.2.2 Robotic Deposition

The fiber and void volume fractions for the robotic fiber head and roller consolidation are summarized in Table 5.

TABLE 5: Average Fiber and Void Fraction Determined at Crossovers, X and Y Positions (Robot)

		X		Y1		Y2		Y3		Beam		Crossover	
		Ave (%)	SD (%)	Ave (%)	SD (%)	Ave (%)	SD (%)	Ave (%)	SD (%)	Ave (%)	SD (%)	Ave (%)	SD (%)
300mm/ min	V_f	33.63	0.16	33.94	0.11	34.47	0.38	34.00	0.21	33.93	0.38	34.32	0.25
	V_v	5.02	0.34	5.13	0.32	4.22	0.40	4.95	0.29	4.87	0.48	9.21	0.27
50mm/ min	V_f	35.91	0.73	35.94	0.46	36.23	0.57	36.48	0.50	36.09	0.65	39.96	0.29
	V_v	2.51	0.55	2.75	0.26	2.25	0.16	2.59	0.23	2.52	0.42	5.89	0.14

The overall results of the fiber and void fraction analysis for the roller consolidation system are promising. For the sample printed at 300 mm/min, the average fiber volume fraction of all the beam sections is approximately 34% and a void volume fraction is below 5%. The crossover sections of this sample show poor consolidation, with only a 34.32% fiber volume fraction and a 9.21% void fraction. For the sample printed at 50 mm/min, the average fiber volume fraction of the beam sections is slightly above 36% with a void volume fraction of just greater than 2.5%. The quality of the crossover sections of this sample was an improvement over that of the higher speed sample, with a fiber volume fraction of 39.96% and a void content of 5.89% by volume.

The most obvious trend is that the fiber volume fraction increased while the void volume fraction decreased when the deposition speed was reduced. This is consistent with additional matrix flow and a longer duration of the applied consolidation. Similar to the reasoning for the crossover geometry being better at the slower speed, the longer time at the elevated temperature resulted in a lower matrix viscosity, improving the flow. Additionally, the slower speed also allows the matrix more time to flow while under the pressure of the consolidation roller. Interestingly, despite the reduced thickness of the Y1 samples, there is no drop in void content for these specimens. The thinner geometry would suggest a higher consolidation pressure on this sample, but there is no obvious influence of this higher pressure on the void content.

4. DISCUSSION

4.1 Geometry Comparison

The compliance difference of the structures of the two automation systems, as well as variations in the initial shaping of the tow between the two systems caused discrepancies in the produced geometry. When analyzing the samples produced with the gantry system, it was observed that there were significant variations in the % Programmed Deviation for the parts printed at 300 mm/min and for those printed at 50 mm/min. This suggests that there is a noticeable difference between the actual and theoretical thickness of the parts. Based on the information shown in figure 9, it is evident that a greater thickness value is observed at both X and Y positions when at 0 for the gantry system. This is due to the sharp angle, leaving the turn of the continuous path, causing tow buckling, which affects the start of the X and Y beam prints. These findings provide valuable insight into the direct digital continuous fiber deposition process and can inform future improvements.

The compliance, due to the spring-loaded print head in the gantry printer, makes predicting the sample thickness difficult. The stiffness of the robotic deposition system generates a more predictable output geometry, as indicated by the consistency between the standard deviations for

each beam at different speeds. However, in both cases, using a Z-position control based on a presumed layer height would require some iteration for the actual thicknesses to match predictions.

The width of the deposited tow is significantly different between the two fiber placement systems. While this was not a parameter that was directly monitored in this study, it is worth discussing. The tow deposited by the gantry system with nozzle consolidation is approximately 50% of the width of the top layer of the tow deposited by roller consolidation using the robotic system. While the tow width is strongly impacted by the applied consolidation force during deposition, the shaping of the deposited tow, prior to consolidation, is different for each system. The gantry deposition system uses a heated zone and a nozzle that initially shapes the flat commingled tow into a cylinder, approximately 1.5 mm diameter, before flattening it under the nozzle. The robotic deposition system heats and consolidates the flat, nominally 6 mm wide, commingled tow without any prior shaping, resulting in the wider resultant consolidated tow. Similarly, the amount of tow spreading at the crossovers is another indication of how the initial shaping of the tow impacts the geometry of the final part. The gantry deposition system spreads the 1.5 mm cylindrical tow to around 7 mm, while the robotic deposition system starts with the flat, unprocessed 6 mm tow and spreads it to approximately 12 mm in the straight sections and about 16 mm at the crossovers. The initial shaping of the tow clearly affects the resulting width of the corresponding samples and limits the ability to further thin the tow with the increased consolidation force at the crossovers.

A similar trend was noted for the geometry of the samples, independent of the placement system used. Generally, the slower deposition rate yielded improved crossover geometry, more consistent with the respective beam thickness, as shown in figures 9 and 10. This is due to the matrix having more time to flow while under the pressure of the nozzle or the consolidation roller. Further, the matrix experiences the heat of the nozzle or consolidation roller for a longer time, allowing more heat transfer into the matrix. This, in turn, lowers the viscosity of the thermoplastic matrix, allowing easier flow to take place. Interestingly, the robotic deposition sample printed at 50 mm/min shows a local minimum at the crossover locations whereas all other samples show a local maximum at the crossover points, as seen in figures 9 and 10. This indicates how the stiffer automation system of the robot, coupled with higher heat in the matrix, can effectively increase the spreading and thinning of the tow.

Both of these systems have demonstrated a capability to generate consistent crossover geometries. The gantry deposition system was able to create a crossover with a maximum thickness increase of 14.38% at 300 mm/min deposition speed. The robotic deposition system was able to create a crossover with a maximum thickness increase of only 8.01% at 300 mm/min deposition rate. Zhao et al. were only able to achieve a minimum height increase of 35% by utilizing the clamp-cut-restart strategy of AFP [4]. Thus, these preliminary results show improved thickness retention over what has been previously reported and does so without the need to cut the continuous fiber at the grid intersections.

4.2 Volume Fraction Comparison

Fiber and void volume fractions are summarized in figure 11. In general, both systems follow many of the same trends. Lower void fractions at the slower speed were measured with both systems. The longer time at the elevated temperature lowered the viscosity of the thermoplastic matrix, easing the flow. Additionally, the slower speed also meant that the matrix had more time

to flow while under the pressure of the nozzle or consolidation roller enabling higher fiber fractions. Higher fiber and void fractions appeared in the crossovers produced by both systems.

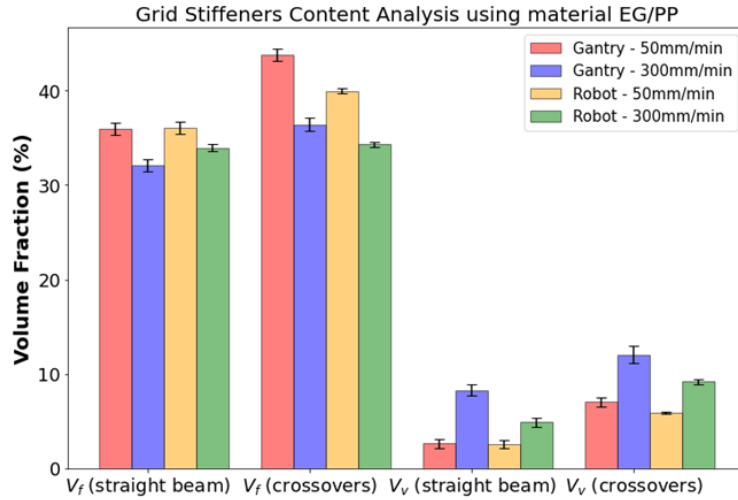


Figure 11: Fiber and void contents of beams and crossovers for Gantry and Robot Deposition.

One source of the increased void fraction could be related to fiber bridging at the crossovers, as suggested in figure 12. Buragohain et al. noted a resin rich area adjacent to the crossover which was due to fiber bridging present in the manufacture of grid stiffened structures. However, Buragohain used a thermoset prepreg and cured those structures in an autoclave, resulting in a resin rich, but low void content volume where fiber bridging is apparent [2].

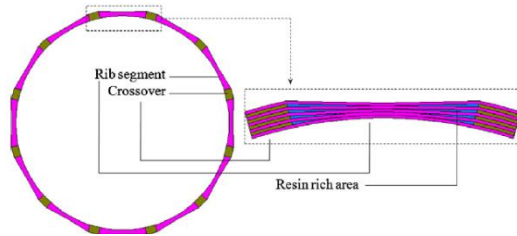


Figure 12: Example of fiber bridging as seen by Buragohain et al. [2]

In the present study, because there is only in-situ consolidation, the fiber bridging present may be more likely to trap voids as the local consolidation force is reduced. Based on the work of Hogan [11], investigating volume fraction variations within the straight beam sections, the fiber volume fraction was found to be lower, and the void volume fraction higher as he traversed toward the lateral edges of the placed tow. Thus, additional micrographic studies would be required to assess the void location and distribution at these crossovers and ultimately determine if voids are concentrated at the fiber bridging.

5. CONCLUSIONS

Both the gantry deposition using a nozzle for consolidation and the robotic deposition with a roller have successfully demonstrated the ability to produce high-quality, continuous fiber, composite grid crossovers with good thickness control at the intersections. The gantry system was able to

achieve thickness deviations lower than 14.38% at the crossovers compared to the straight grid sections while the robotic system was able to achieve thickness deviations less than 8.01% at the crossovers. Although both systems are capable of minimizing thickness build-up at the crossovers, the roller deposition head on the robot, being mounted on a stiffer automation system, seems to be able to produce a more consistent geometry at varying speeds. Both systems can produce low void, high volume fraction continuous fiber reinforced composite grid stiffeners, particularly at low speeds, all with radically reduced tooling.

6. ACKNOWLEDGMENT

This material is based upon work supported by the U.S. Department of Energy's Office of Energy Efficiency and Renewable Energy (EERE) under the Advanced Manufacturing Office, Award Number DE-EE0009404. The views expressed herein do not necessarily represent the views of the U.S. Department of Energy or the United States Government.

7. REFERENCES

- [1] S.M. Huybrechts, S.E. Hahn and T.E. Meink, *Grid Stiffened Structures: A Survey of Fabrication, Analysis and Design Methods*, ICCM/12, 1999.
- [2] C. Zhao, M.J. Donough, B.G. Prusty and J. Xiao, *Influences of Ply Waviness And Discontinuity On Automated Fiber Placement Manufactured Grid Stiffeners*. *Composite Structures* 256, 2021.
- [3] S.M. Huybrechts, T.E. Meink, P.M. Wegner and J.M. Ganley, *Manufacturing Theory For Advanced Grid Stiffened Structures*. *Composites Part A: Applied Science and Manufacturing* 33.2, pp. 155-161, 2002.
- [4] M. Buragohain, and R. Velmurugan, *Study Of Filament Wound Grid-Stiffened Composite Cylindrical Structures*, *Composite Structures*, Volume 93, Issue 2, 2011,
- [5] Y.G. Lee, J.H. Choi, M.J. Lee and S.M. Kim, *Compressive Strength Stabilizing Manufacturing Method Of Anisogrid Composite Structure Ribs Without An Outer Skin*. *Compos. Part B Eng.*, vol. 203, Dec. 2020.
- [6] H. Ahmadi and G. Rahimi, *Analytical and experimental investigation of transverse loading on grid stiffened composite panels*, *Compos. Part B Eng.*, vol. 159, pp. 184–198, Feb. 2019.
- [7] S. Shroff, E. Acar and C. Kassapoglou, *Design, Analysis, Fabrication, And Testing Of Composite Grid-Stiffened Panels For Aircraft Structures*. *Thin-Walled Struct.*, 2017.
- [8] Z. Qureshi, T. Swait, R. Scaife and H.M. El-Dessouky, *In Situ Consolidation of Thermoplastic Prepreg Tape Using Automated Tape Placement Technology: Potential And Possibilities*. *Compos. Part B Eng.*, 2014.
- [9] G. Gardiner, *Integrating Antennas Into Composite Aerostructures*, *Composites World*, 2021.
- [10] P.A. Rodriguez, *Dynamic Mechanical Analysis For Quality Evaluation Of Additively Manufactured Continuous Fiber Reinforced Thermoplastic Matrix Composites Subject To Manufacturing Defects*, Master's Thesis, Colorado State University, 2019.
- [11] S.J. Hogan and D.W. Radford, *Direct Digital Manufacture of Continuous Fiber Reinforced Thermoplastic High Aspect Ratio Composite Grid Stiffeners with Radically Reduced Tooling*, CAMX'22, Anaheim, California, United States, 2022.
- [12] S.J. Hogan, *Direct Digital Manufacture of Continuous Fiber Reinforced Thermoplastic High Aspect Ratio Grid Stiffeners and Grid Stiffener Intersections with Radically Reduced Tooling*, Master's Thesis, Colorado State University, 2023.

- [13] K.M. Warlick and D.W. Radford, *Tow Positional Fidelity In A Continuous Fiber/3D Printing Approach On A Curved Surface*. CAMX'17, Orlando, Florida, 2017.
- [14] M.E. Bourgeois, M.E., and D.W. Radford, *Out of Plane Placement of Tensioned Commingled Roving Creating Truss Sandwich Panels*. CAMX, 2019, Dallas. Texas, 2019.
- [15] *ASTM D792-20*; Standard Test Methods for Density and Specific Gravity of Plastics. ASTM International: West Conshohocken, PA, USA, 2020.
- [16] *ASTM D3171-15*; Standard Test Methods for Constituent Content of Composite Materials. ASTM International: West Conshohocken, PA, USA, 2015.
- [17] A. Gleadall, *FullControl GCode Designer: Open-Source Software for Unconstrained Design in Additive Manufacturing*, Additive Manufacturing, vol. 46, 2021.